3708–3721 *Nucleic Acids Research, 2006, Vol. 34, No. 13*
doi:10.1093/nar/gkl459

Characterization of RNA sequence determinants and antideterminants of processing reactivity for a minimal substrate of *Escherichia coli* ribonuclease III

Alexandre V. Pertzev and Allen W. Nicholson*

Department of Chemistry, Temple University, Philadelphia, PA 19122, USA

Received January 17, 2006; Revised June 14, 2006; Accepted June 15, 2006

ABSTRACT

Members of the ribonuclease III family are the primary agents of double-stranded (ds) RNA processing in prokaryotic and eukaryotic cells. Bacterial RNase III orthologs cleave their substrates in a highly site-specific manner, which is necessary for optimal RNA function or proper decay rates. The processing reactivities of *Escherichia coli* RNase III substrates are determined in part by the sequence content of two discrete double-helical elements, termed the distal box (db) and proximal box (pb). A minimal substrate of *E.coli* RNase III, μR1.1 RNA, was characterized and used to define the db and pb sequence requirements for reactivity and their involvement in cleavage site selection. The reactivities of μR1.1 RNA sequence variants were examined in assays of cleavage and binding *in vitro*. The ability of all examined substitutions in the db to inhibit cleavage by weakening RNase III binding indicates that the db is a positive determinant of RNase III recognition, with the canonical UA/UG sequence conferring optimal recognition. A similar analysis showed that the pb also functions as a positive recognition determinant. It also was shown that the ability of the GC or CG bp substitution at a specific position in the pb to inhibit RNase III binding is due to the purine 2-amino group, which acts as a minor groove recognition antideterminant. In contrast, a GC or CG bp at the pb position adjacent to the scissile bond can suppress cleavage without inhibiting binding, and thus act as a catalytic antideterminant. It is shown that a single pb+db 'set' is sufficient to specify a cleavage site, supporting the primary function of the two boxes as positive recognition determinants. The base pair sequence control of reactivity is discussed within the context of new structural information on a post-catalytic complex of a bacterial RNase III bound to the cleaved minimal substrate.

INTRODUCTION

Ribonucleases are a structurally and mechanistically diverse group of enzymes with essential roles in RNA maturation, RNA decay, gene regulation and host defense (1). Ribonucleases involved in RNA processing are highly selective *in vivo*, and can function in a coordinated manner in multistep maturation and degradation pathways (2–6). The substrate selectivity and cleavage site specificity are necessary for the correct operation of RNA maturation and decay pathways, and to prevent inappropriate cleavage of other RNAs. Double-stranded (ds) RNA structures are functionally important targets of enzymatic cleavage, and are recognized by members of the ribonuclease III family of endoribonucleases (7–11). In bacterial cells, RNase III cleavage of dsRNA is a key step in the maturation and degradation of coding and noncoding RNAs, and can regulate gene expression by controlling RNA stability and translational efficiency (3,7). In eukaryotic cells the RNase III orthologs Dicer and Drosha participate in the maturation of microRNAs—small noncoding RNAs that regulate gene expression (12–16). Dicer also initiates RNA interference and related gene silencing pathways by processing dsRNA structures to short interfering (si) RNAs, that in turn target homologous RNA sequences for enzymatic destruction (12,14,17,18). The action of Dicer underscores the functional flexibility of RNase III orthologs in their ability to cleave cellular substrates in a highly site-specific manner, while processing dsRNAs of broad sequence content to short products.

Bacterial RNase III orthologs are the structurally simplest family members, and consist of a polypeptide of ~220 residues, containing an N-terminal nuclease domain and a C-terminal dsRNA-binding domain (dsRBD) (3,7,9,19,20). The latter domain consists of a single copy of the conserved dsRNA-binding motif (dsRBM), which is present in many other proteins that recognize dsRNA (21–24). Since bacterial RNase III orthologs function as homodimers, the holoenzyme

*To whom correspondence should be addressed. Department of Chemistry, Temple University, 1901 North 13th Street, Philadelphia, PA 19122, USA. Tel: +1 215 204 9048; Fax: +1 215 204 1532; Email: anichol@temple.edu

contains two dsRBDs. A typical target site in a bacterial RNase III substrate is cleaved on both strands, creating 2 nt 3′-overhangs and 5′-phosphate, 3′-hydroxyl product termini (25,26). In a proposed reaction pathway for bacterial RNase III (20), one of the two dsRBDs recognizes a correctly-sized substrate, which is then engaged by the nuclease domain and the second dsRBD to create the catalytically competent complex (20).

Cleavage sites of bacterial RNase III substrates are determined by specific RNA structural and sequence elements, also referred to as reactivity epitopes. Helix length is a primary reactivity epitope, with substrates of *Escherichia coli* RNase III typically exhibiting two helical turns (3,7,9,25,26). The coaxial stacking of short helices can provide a quasi-continuous helix of sufficient length to allow cleavage (27). However, the shortest helix that confers appreciable reactivity under standard conditions has not been defined for any bacterial RNase III ortholog. Other structure-based reactivity epitopes include internal loops or bulges, which can limit cleavage of a target site to a single phosphodiester (3,7,25–27). This pattern of cleavage provides 3′-hairpin stem–loop structures that can protect the processed RNA from 3′–5′ exonucleolytic digestion (3,7,28). A bulge-helix-bulge motif has been identified that can permit binding of *E.coli* RNase III, but inhibits cleavage (29). The existence of an 'uncoupling' motif supports genetic (30) and structural (20) evidence that *E.coli* RNase III can regulate gene expression as an RNA-binding protein.

Base pair sequence elements also participate in controlling substrate reactivity, and may also be involved in target site selection. While a sequence alignment analysis of *E.coli* RNase III substrates (31) did not identify any conserved sequences that could act as positive recognition determinants, it was observed that specific base pair sequences are excluded from two discrete double-helical segments, termed the proximal box (pb) and distal box (db) (32). Introduction of one or more of the excluded base pairs into either box within a model substrate inhibited cleavage by *E.coli* RNase III, with the inhibition due to an interference with enzyme binding (32). Based on these findings it was proposed (3,32) that *E.coli* RNase III cleavage sites are determined by a default mechanism, in which the reactive site is identified by the absence of inhibitory base pairs within the pb and db, and with the other phosphodiesters effectively protected by inhibitory base pairs in the corresponding pb and db positions. This mechanism served to rationalize the ability of bacterial RNase III to degrade long dsRNAs of broad sequence content to short duplex products in a largely base pair-sequence-independent manner, while carrying out site-specific cleavage of cellular substrates. This mechanism of cleavage site selection does not involve positive sequence recognition determinants. Nonetheless, such elements may exist, and could be nonobvious features of the diverse substrates for bacterial RNases III. To more precisely define the role of base pair sequence in controlling processing reactivity and target site selection, we present here an analysis of a minimal substrate of *E.coli* RNase III. We show that specific base pair sequence elements function as positive recognition determinants. In addition, two functional classes of negative determinants (antideterminants) are defined that either inhibit recognition, or suppress cleavage without affecting recognition. The RNA sequence-reactivity correlations are discussed in reference to the recently-reported structure of a bacterial RNase III bound to a cleaved minimal substrate.

MATERIALS AND METHODS

Materials

Water was deionized and distilled. Chemicals and reagents were molecular biology grade and were purchased from Sigma–Aldrich or Fisher Scientific. Ribonucleoside 5′-triphosphates were obtained from Amersham–Pharmacia Biotech. About 3000 Ci/mmol of [γ-^{32}P]ATP was purchased from Perkin–Elmer. *E.coli* bulk stripped tRNA was purchased from Sigma and was further purified by repeated phenol extraction followed by ethanol precipitation. T4 polynucleotide kinase was purchased from New England Biolabs, and calf intestine alkaline phosphatase was obtained from Roche Molecular Biochemicals. T7 RNA polymerase was purified in-house as described (33). $(His)_6$-RNase III was purified as described (34). The catalytic behavior of $(His)_6$-RNase III (referred to in this study as RNase III) are essentially the same as the native enzyme (34). Oligodeoxynucleotide transcription templates were synthesized by Invitrogen and were purified by denaturing gel electrophoresis, followed by chromatography on DEAE–Sepharose (34,35). Purified DNAs were stored at -80° in Tris–EDTA buffer (pH 8).

Substrate preparation

RNAs were enzymatically synthesized *in vitro* using oligodeoxynucleotide templates and T7 RNA polymerase according to an established protocol (36) with modifications as described (34). The sequences of the DNA oligonucleotide transcription templates are available upon request. For 5′ ^{32}P-labeling, enzymatically synthesized RNA ($\sim$300 pmol) was treated with calf intestine alkaline phosphatase (6 U) at 37° for 30 min in buffer consisting of 50 mM Tris–HCl (pH 8.5) and 0.1 mM EDTA. The RNA was purified by phenol–chloroform extraction and ethanol precipitation. Dephosphorylated RNA (40–65 pmol) was incubated at 37°C for $\sim$30 min with 5–10 μCi of [γ-^{32}P]ATP (3000 Ci/mmol) and T4 polynucleotide kinase (10 U), using the supplied buffer. The radiolabeled RNA was purified by electrophoresis in a 15% polyacrylamide gel containing TBE buffer and 7 M urea, followed by final purification by DEAE–Sepharose chromatography (35). RNA was stored at -20° in Tris–EDTA (pH 7) buffer. RNAs also were synthesized by Dharmacon Research Inc., using 2′-ACE-protected phosphoramidites. Synthetic RNAs were deprotected using the supplied reagents, and were further purified by denaturing gel electrophoresis followed by DEAE–Sepharose chromatography. Chemically synthesized RNAs were 5′ ^{32}P-labeled according to the protocol described above, but omitting the phosphatase step. The amount of RNA or DNA was determined by ultraviolet (UV) absorbance, using reported (37) molar extinction coefficients (260 nm, $M^{-1}cm^{-1}$) as follows: A, 15 400; G, 11 500; C, 7400; U, 10 000; T, 8700; Inosine (I), 11 000; 2-aminopurine (2AP), 1000 and 2,6-diaminopurine (DAP), 10 200.

Substrate cleavage assay

Cleavage assays were carried out essentially as described (34) with some modification. Reactions were performed using 5′ ^{32}P-labeled substrate in buffer consisting of 160 mM NaCl, 30 mM Tris–HCl (pH 8), 0.1 mM EDTA, 0.1 mM DTT, tRNA (0.01 mg/ml) and 5% glycerol (v/v). Reactions were initiated by adding $MgCl_2$ (10 mM final concentration) and incubated at 37°C (see Figure legends and Table legends for additional specific conditions). Short reaction times limited conversion of substrate to product. Reactions were quenched by addition of excess EDTA (20 mM final concentration) and the samples electrophoresed (25 V/cm) at room temperature in a 15% polyacrylamide gel (29.2/0.8 acrylamide/bisacrylamide), containing TBE buffer and 7 M urea. The gel assays were visualized by phosphorimaging (Typhoon 9400 system) and analyzed by ImageQuant software. Reactions were performed at least in duplicate, and average values are reported. Figure and Table legends provide additional details on specific assays.

Gel mobility shift assay

Gel shift assays were carried out essentially as described (34). In these assays Mg^{2+} was replaced by Ca^{2+}, which promotes substrate binding to RNase III while preventing substrate cleavage (38). Briefly, 5′ ^{32}P-labeled RNA was heated in a boiling water bath for ~30 s, then snap-cooled on ice. The RNA was incubated at 37°C for 10 min with RNase III in buffer consisting of 160 mM NaCl, 10 mM $CaCl_2$, 30 mM Tris–HCl (pH 8), 0.1 mM EDTA, 0.1 mM DTT, 5 μg/ml tRNA and 5% glycerol (v/v). The binding reactions were placed on ice for ~20 min, then electrophoresed (6 V/cm) at 5–6°C in a 6% nondenaturing polyacrylamide gel (80:1 acrylamide:bisacrylamide) containing 0.5× TBE buffer and 10 mM $CaCl_2$. Binding reactions were visualized by phosphorimaging and quantitated using Imagequant software (34). Apparent dissociation constants (K_D' values) of the RNA–protein complexes were determined as described (38,39), and involved measurement of the amount of free (unbound) substrate as a function of RNase III concentration. This method provides K_D' values for RNA–protein complexes that cannot be directly observed as discrete complexes in nondenaturing polyacrylamide gels (39).

RESULTS

Characterization of μR1.1 RNA: a minimal substrate of *E.coli* RNase III

We sought to identify an *E.coli* RNase III substrate that would contain the minimal set of sequence and structural elements needed for efficient binding and cleavage. A minimally-sized substrate is expected to be sensitive to changes in sequence or structure, thus facilitating the characterization of reactivity epitopes. A time course for cleavage of R1.1[WC] RNA (3,32) (structure shown in Figure 1A) yielded two intermediates, with each species resulting from cleavage of one of the two target site phosphodiesters (site 1 or site 2; Figure 1A). It was noted that the site-2-cleaved intermediate in isolated form can be cleaved at site 1 at a rate comparable to that of the parent substrate (3). Based on this observation, substrates were prepared that were based on the site-2-cleaved R1.1[WC] RNA intermediate, and that contained either a shortened double-helical stem or a shortened 5′ single-strand extension (Figure 1A). The cleavage reactivities of the RNAs were determined under standard conditions (see Materials and Methods). To allow detection of any changes in reactivity due to either an altered binding affinity or an altered catalytic rate, the enzyme and substrate concentrations were significantly less than the K_m for μR1.1 RNA (see below). A high enzyme/substrate ratio provided single-turnover kinetics, and the extent of cleavage was measured at short times, in which only a limited amount of substrate was converted to product. These conditions allowed determination of the relative reactivity, defined as the fraction of a variant that is cleaved divided by the fraction cleaved of a reference substrate (μR1.1 RNA; see Figure 1A and also below), determined under identical conditions.

Representative cleavage assays, shown in Figure 1A, demonstrate that substrate reactivity is sensitive to helix length. Thus, deletion of a single base pair from the top of the stem (μR1.1[Δ1] RNA, Figure 1A) causes a 50-fold drop in reactivity, while deletion of 2 bp (μR1.1[Δ2] RNA, Figure 1A) essentially abolishes cleavage. Gel shift assays of the two shortened μR1.1 RNA variants (assays not shown; see Figures 2B and 4 for representative experiments) reveal that the diminished reactivities are due to a loss of RNase III binding affinity. We conclude that an 11 bp helix between the cleavage site and tetraloop represents the shortest length that provides significant reactivity. Also, the comigration of the 5′ end-containing cleavage products of μR1.1 RNA and μR1.1[Δ1] RNA (Figure 1A, lanes 6 and 8), establish that the base pair deletions do not alter the site of cleavage. In this regard, the 15% denaturing polyacrylamide gels used here can detect single-nucleotide differences in lengths of short [(≤~10 nt) cleavage products (32,40); data not shown]. Shortening the sequence between the cleavage site and the 5′ end to 6 nt does not significantly affect cleavage reactivity (relative reactivities of μR1.1[5′ + 2] RNA and μR1.1 RNA are 1.26 and 1.0, respectively; Figure 1A). However, a further reduction in length strongly reduces reactivity (data not shown). The steady-state kinetic parameters for μR1.1 RNA were determined by measuring the initial rate as a function of substrate concentration. A best-fit curve to a Michaelis–Menten kinetic scheme (Figure 2A) yielded a K_m of 148 nM and a k_{cat} of 2 min^{-1}. Based on these data we conclude that the 34 nt μR1.1 RNA represents a minimal substrate for *E.coli* RNase III. A gel shift assay (Figure 2B) reveals that μR1.1 RNA binds RNase III to form a complex with a measured apparent dissociation constant (K_D') of 205 nM (Figure 2C). Although the gel shift assay cannot directly provide stoichiometric information, the observation of a single shifted band is consistent with the formation of a 1:1 protein–RNA complex.

The scissile phosphodiester is not determined by tetraloop position or sequence

μR1.1 RNA exhibits a GCAA tetraloop, which belongs to the GNRA family of tetraloops that stabilize stem–loop structures (41). We sought to determine whether the tetraloop sequence or position participates in cleavage site selection.

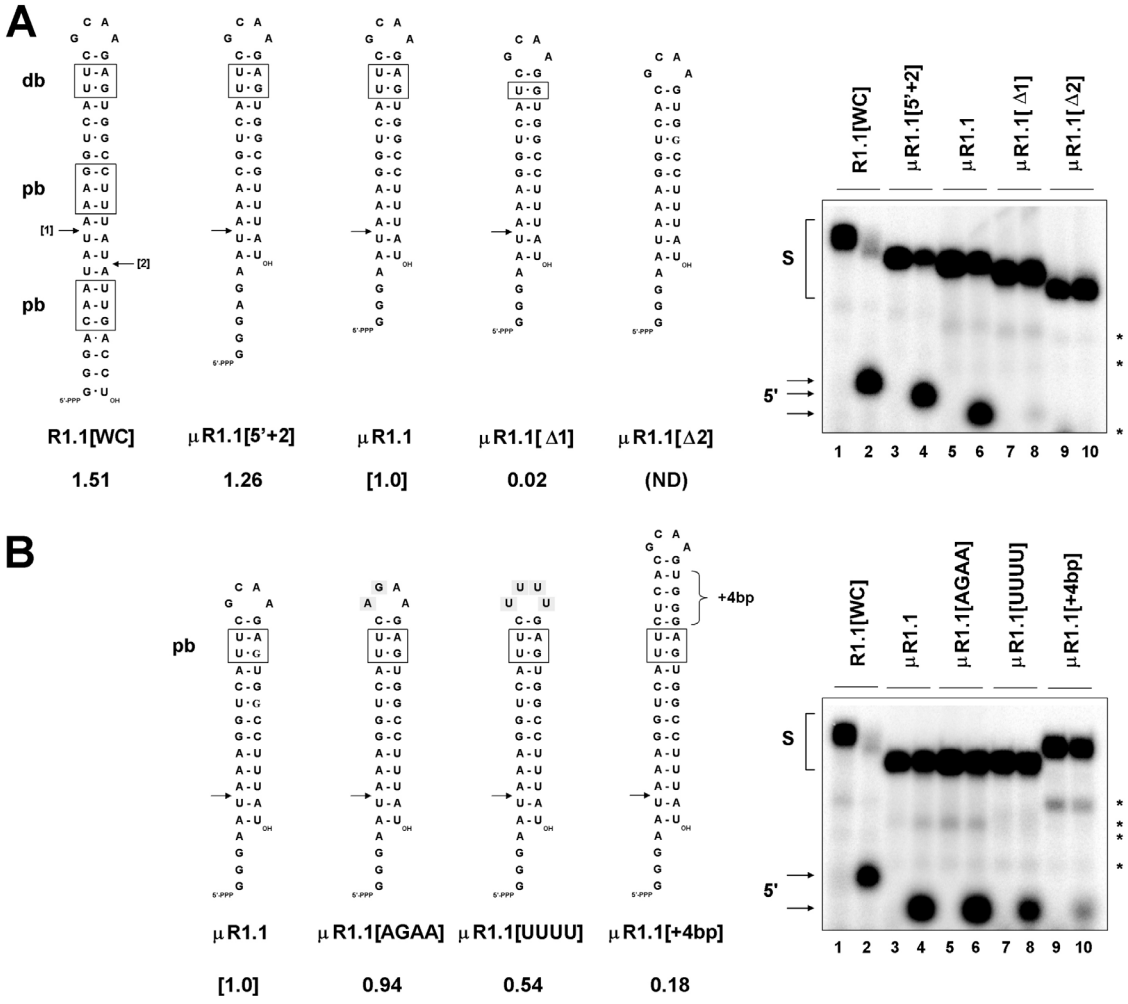

Figure 1. Identification and characterization of a minimal substrate of *E.coli* RNase III. (**A**) Sequence and secondary structure of R1.1[WC] RNA and smaller variants, including μR1.1 RNA. The scissile bonds in R1.1[WC] RNA are indicated ([1] and [2]), and the db and two pb are outlined. Time course assays of cleavage were performed using ~2.5 nM 5′ ^{32}P-labeled RNA, 10 nM RNase III and buffer containing 10 mM Mg^{2+} (see Materials and Methods). In the gel electropherogram shown on the right, lanes 1, 3, 5, 7 and 9 represent incubation of substrate for 4 min with RNase III in the absence of Mg^{2+}, while lanes 2, 4, 6, 8 and 10 show complete reactions. 'S' and '5′' refer to the uncleaved substrates and 5′ end-containing cleavage products, respectively. The asterisks indicate minor products of nonspecific, nonenzymatic cleavages. The relative reactivities are provided below the RNA structures, and represent the average of three or more independent experiments, with the standard error of the mean of ±9%. The cleavage of μR1.1[Δ2] RNA was not detectable (ND), so a relative reactivity could not be determined. Since μR1.1 RNA is the reference substrate (see Results), its relative reactivity is 1.0. The μR1.1 RNA cleavage site was mapped by comparison of the gel electrophoretic mobilities of the products of cleavage of internally ^{32}P-labeled μR1.1 RNA with the cleavage products of R1.1[WC] RNA (data not shown). This experiment demonstrated the comigration of the 28 bp upper stem–loop products, created by cleavage at sites 1 and 2; see also (32). (**B**) Examination of the involvement of the tetraloop as a reactivity epitope. In the gel electropherogram on the right, lanes 1, 3, 5, 7 and 9 represent incubation of substrate for 4 min with RNase III in the absence of Mg^{2+}, while lanes 2, 4, 6, 8 and 10 represent complete reactions. 'S' and '5′' refer to uncleaved substrate and 5′ end-containing cleavage product, respectively. The asterisks indicate minor products of nonspecific, nonenzymatic cleavage. The relative reactivities are provided below the RNA structures, and are the average of three or more independent experiments, with the average standard error of the mean of ±9%.

In this regard, cleavage sites of hairpin substrates of the yeast RNase III ortholog Rnt1p are determined by their distance (~14–16 bp) from a conserved RGNN tetraloop (8,9). A μR1.1 RNA variant was prepared that contains a 4 bp insertion between the db and the GCAA tetraloop (μR1.1[+4 bp] RNA). This variant is cleaved at the canonical site, as indicated by the comigration of the 5′ end-containing cleavage product with that of μR1.1 RNA (Figure 1B, compare lanes 4 and 10). Thus, changing the position of the tetraloop does not change the cleavage site. However, the reactivity of (μR1.1[+4 bp] RNA is ~5-fold lower than the parent substrate (see also below). To determine whether the tetraloop sequence determines the cleavage site or affects reactivity, two μR1.1 RNA variants were prepared that contained either an AGAA tetraloop (which conforms to the RGNN motif of yeast Rnt1p substrates) or a UUUU tetraloop. A cleavage assay (Figure 1B, compare lanes 6 and 8 with lane 4) shows that the two variants retain comparable activity as the parent substrate, and are cleaved at the canonical site. Thus, there is no strict tetraloop sequence requirement for reactivity.

The db functions as a positive recognition determinant

The cleavage reactivities were determined for a set of μR1.1 RNA variants that exhibited the full range of base pair

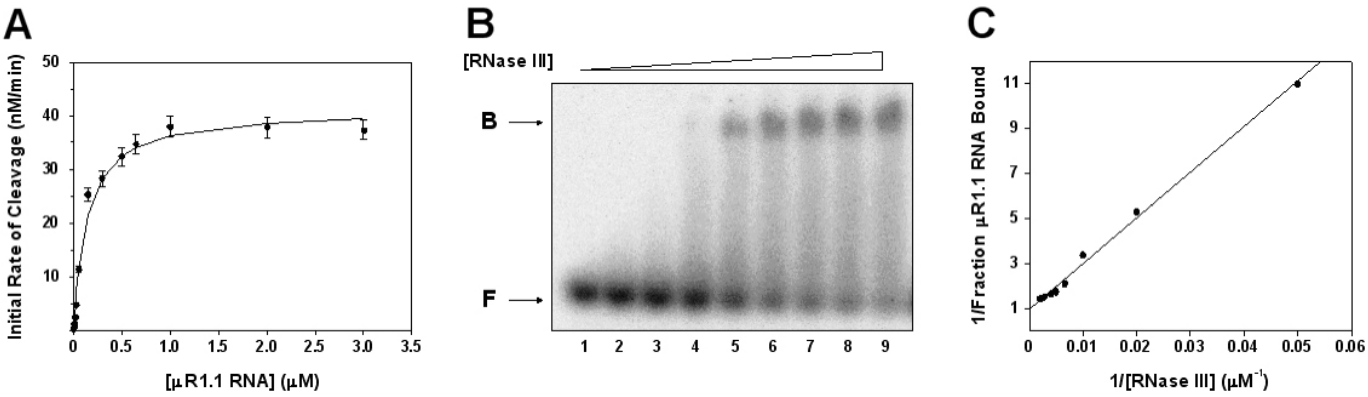

Figure 2. Substrate behavior of μR1.1 RNA. (**A**) Determination of steady-state kinetic parameters. The initial rate of cleavage of μR1.1 RNA was determined as a function of substrate concentration. The best-fit curve to a Michaelis–Menten scheme is shown, with each point representing the average of at least three experiments. The K_m is 148 ± 21 nM, and the k_{cat} is 2.1 min^{-1}. (**B**) Gel mobility shift assay of μR1.1 RNA-binding to RNase III. The assay was performed as described in Materials and Methods, using 5′ ^{32}P-labeled RNA, and Ca^{2+} (10 mM) in place of Mg^{2+}. The RNase III concentrations in the reactions shown in lanes 1–9 are: 0, 20, 50, 100, 150, 200, 250, 350 and 500 nM, respectively. 'F' and 'B' refer to free and bound μR1.1 RNA, respectively. The smear of radioactivity between the free and bound RNA in lanes 4–9 represents partial dissociation of the complex during electrophoresis (39). (**C**) Determination of the apparent dissociation constant, K'_D. The reciprocal of the fraction of substrate bound was plotted versus the reciprocal of the RNase III concentration. A simple bimolecular equilibrium provides a linear relation (39,54), with a *y*-intercept of 1 and a slope corresponding to the K'_D, which is 205 nM (see also Results).

substitutions at each position in the helical stem. The measured relative reactivities reveal three discrete double-helical regions, within which base pair substitution significantly affects reactivity (Figure 3). One region corresponds to the db, in which it is seen that all substitutions significantly reduce (>∼5-fold) cleavage reactivity (Figure 3). In particular, there is a stringent requirement for a UG pair in the second position. Here, a UG→GU substitution causes a 50-fold reduction in reactivity, while the UG→AU substitution causes a >30-fold reduction in reactivity (Figure 3). The effect of the latter substitution is consistent with the substrate alignment analysis that revealed an exclusion of the AU pair from this position (32). Based on the comigration of the 6 nt, 5′ end-containing cleavage products (gel electropherograms not shown), none of the db substitutions alter the cleavage site. The binding affinities of the db variants were assessed by gel shift assays. Figure 4A shows representative assays and provides the K'_D values for a subset of the μR1.1 RNA variants, and Figure 4B demonstrates a correlation of cleavage reactivity with binding affinity. Based on this correlation, and the stringent sequence requirement we conclude that the db functions as a positive determinant of recognition, with the canonical UA/UG sequence providing optimal function in binding RNase III.

The pb is a positive recognition determinant, and a site of catalytic antideterminant action

The base pair substitution analysis (Figure 3) establishes the pb as a 4 bp element, with each position exhibiting specific sequence requirements for optimal cleavage reactivity. Gel shift assays were performed and the K'_D values determined (Table 1). The data shows that base pair substitutions at pb positions 1, 2 and 3 inhibit RNase III binding. The particularly strong inhibitory effect on binding of the CG or GC bp at pb position 2 was examined further. Since Watson–Crick base pairing is formally retained with either substitution, the decreased reactivity suggests an involvement of one or more base functional groups. To assess this, the guanine of the inhibitory CG bp was changed to inosine (I). The CI pair lacks the purine C2 exocyclic amino group, but retains two standard hydrogen bonds, and therefore is not expected to disrupt secondary structure. A cleavage assay (Figure 5A, middle panels) reveals that μR1.1[C_9:I_{30}] RNA has a relative reactivity of 0.33, which is ∼5-fold greater than that of μR1.1[C_9:G_{30}] RNA, but is only 3-fold less than that of μR1.1 RNA. Thus, removal of the purine 2-amino group restores the majority of the cleavage reactivity. We also examined the consequences of introducing a 2-amino group into the functionally innocuous UA bp. Thus, while μR1.1[U_9:A_{30}] RNA exhibits a relative reactivity of 0.8, substitution of A_{30} with DAP reduces the relative reactivity by ∼25-fold (Figure 5B, middle panels). A gel shift assay (Figure 5B, lower panels) shows that the DAP-containing variant exhibits a low affinity for RNase III, similar to μR1.1[C_9:G_{30}] RNA. Based on the analysis of the inosine- and DAP-containing variants we conclude that the purine 2-amino group at pb position 2 is primarily responsible for inhibition of RNase III binding. Moreover, the low reactivity of μR1.1[G_9:C_{30}] RNA (Figure 3) suggests that the purine 2-amino group does not need to occupy a precise position in the minor groove in order to confer inhibition. To assess the involvement of the guanine 6-keto group in inhibition, 2-aminopurine (2AP) was inserted in place of G_{30} in μR1.1[C_9:G_{30}] RNA. The 2AP-containing variant has a relative reactivity (0.05) that is essentially unchanged with respect to that of μR1.1[C_9:G_{30}] RNA (relative reactivity 0.06) (gel electropherograms not shown). Thus, the guanine 6-keto group does not appear to contribute to the inhibitory action of the CG bp at pb position 2. However, it should be noted that removal of the 6-keto group would formally create a wobble pair, which itself could cause inhibition through a local structural effect.

Base pair substitutions at pb position 4 affect μR1.1 RNA reactivity in a qualitatively different manner than substitutions at pb positions 1–3. Thus, the AU→GC and AU→CG

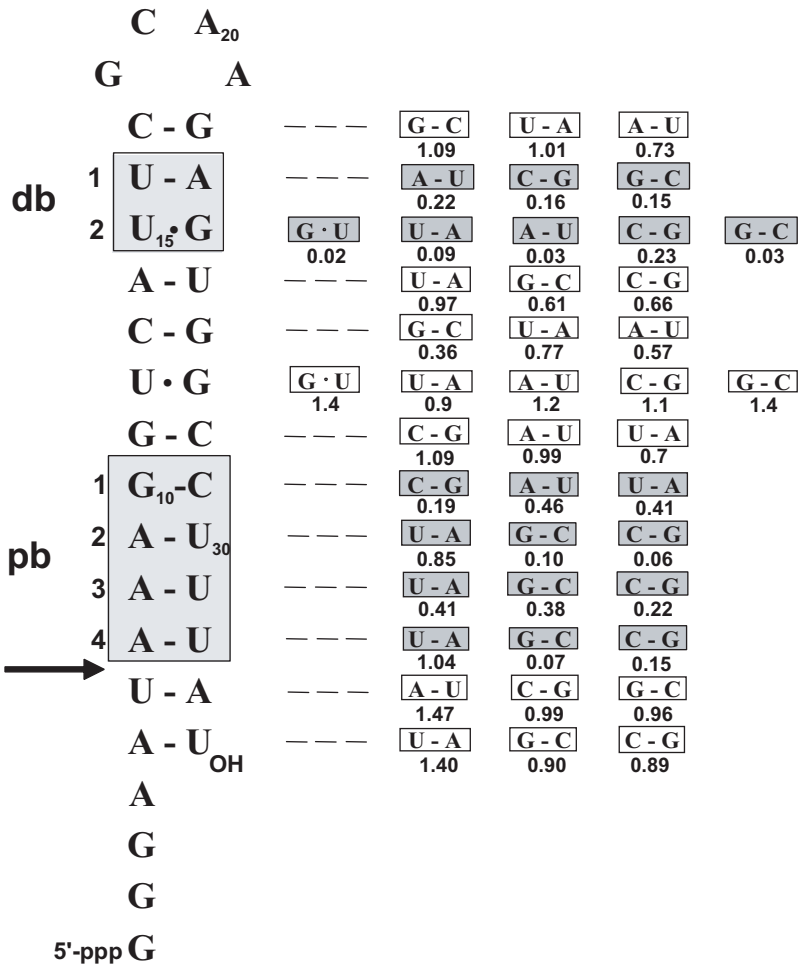

Figure 3. Base pair sequence effects on μR1.1 RNA cleavage reactivity. The diagram shows the sequence and proposed secondary structure of μR1.1 RNA. The arrow indicates the RNase III cleavage site, and the pb and db are also indicated. The numbers (1–4) to the left of the two boxes refer to the specific subsites within each box. On the right are shown the base pair substitutions. The relative reactivity is provided below each substitution, and represents the average of three experiments, with a standard error of the mean of ±15%.

substitutions cause 14- and 7-fold reductions in cleavage reactivity, respectively (Figure 3), but do not inhibit substrate binding, as indicated by the similar K'_D values (Table 1). The GC or CG bp therefore function as catalytic antideterminants, which suppress cleavage without affecting substrate binding (29). If the inhibition is due to the increased strength of the GC or CG bp compared to the canonical AU (or UA) bp, then reactivity should be restored upon substitution of guanine by inosine, which would reduce the number of hydrogen bonds from 3 to 2. In fact, the GC→IC substitution enhances cleavage reactivity by ∼3-fold (Table 2; cleavage assays not shown), suggesting that base pair strength is a contributing factor. However, the reactivity of the inosine-containing variant is still ∼4-fold lower than that of μR1.1 RNA (Table 2), indicating that additional features of the CG or GC bp contribute to inhibition of cleavage (see also Discussion).

A db+pb set is sufficient to specify a cleavage site

If the db and pb are positive recognition determinants, then introduction of an additional db+pb 'set' into the minimal substrate would specify a new target site. To test this we prepared a substrate that contains two db+pb sets. R1.1[db1pb1,db2pb2] RNA (Figure 6) is based on μR1.1 RNA[+4 bp] RNA (see Figure 1), but includes an extended stem below the target sites in order to minimize any effects of the helix terminus on reactivity. The db1pb1 pair corresponds to that of μR1.1 RNA, with db1 directly adjacent to the tetraloop. Given the overlapping positions of the two db+pb sets it is expected that there would be mutually exclusive recognition by RNase III of the two sets. A cleavage assay reveals that 5′ ^{32}P-labeled R1.1[db1pb1,db2pb2] RNA is cleaved at the site specified by db1pb1 (site 1), and also at the site specified by db2pb2 (site 2), albeit with lower efficiency (Figure 6C, lane 2). Thus, the introduction of a second db+pb site creates a new target site. Sequencing gel analysis of the cleaved products (gel electropherogram not shown) confirmed the positions of the cleavage sites determined by each db+pb set. Given the lower reactivity of μR1.1 RNA[+4 bp] RNA (Figure 1), cleavage of the target site specified by db2pb2 (where db2 also is 4 bp from the tetraloop) is expected to be less efficient than cleavage of the target site specified by db1pb1. A significant reduction in cleavage at site 1 is observed when an inhibitory base pair substitution

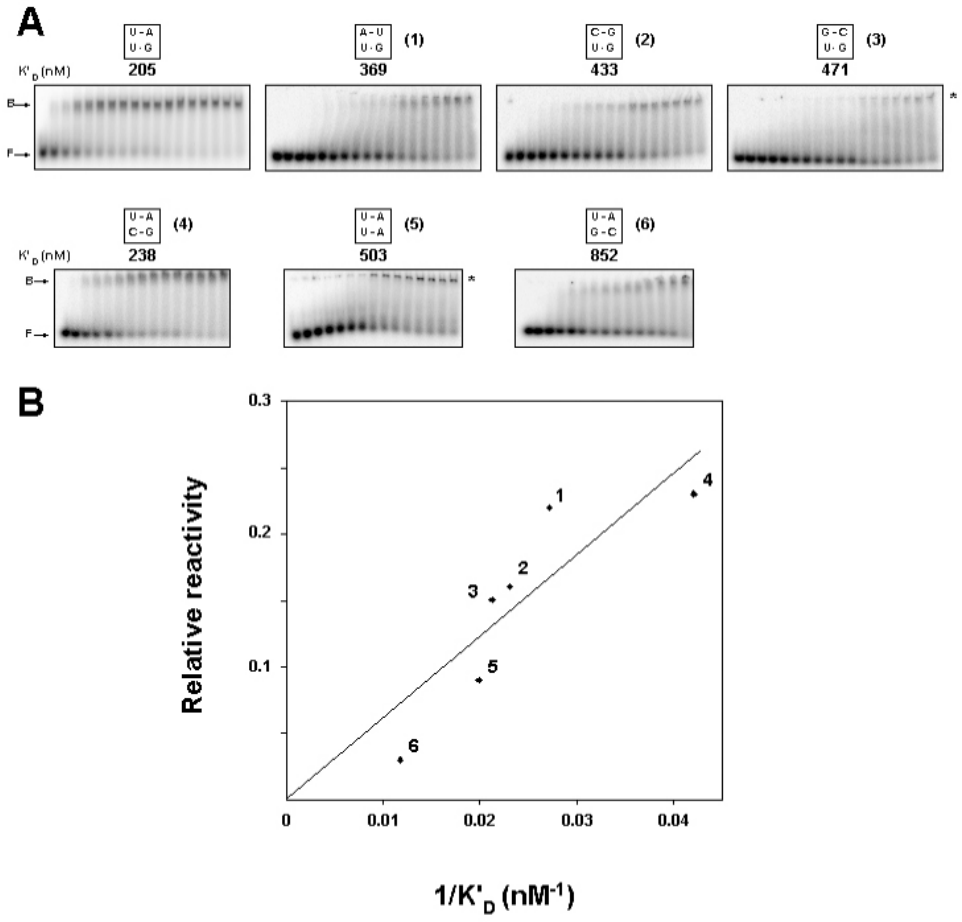

Figure 4. Gel shift assays of db sequence variants of μR1.1 RNA. (**A**) Gel shift assays. Assays were performed as described in Materials and Methods. The K'_D values are provided below each db sequence. The first lane in each panel shows a binding reaction in the absence of RNase III. Lanes 2–18 in the upper row panels and lanes 2–15 in the lower row panels represent RNase III concentrations of 50, 100, 150, 200, 250, 300, 350, 400, 450, 500, 650, 800, 950, 1500, 2000, 2500 and 3000 nM; and 50, 100, 150, 200, 250, 300, 400, 550, 700, 850, 1000, 1500, 2000 and 2500 nM, respectively. (**B**) Correlation between binding affinity and cleavage reactivity of db sequence variants. The relative reactivities of five variants [denoted 1–5 in (A)] were plotted versus the reciprocal of the apparent dissociation constants. The wild-type point is not shown on the graph, but has a $1/K'_D$ (K'_D) of 4.9×10^{-2}nM^{-1} and a relative reactivity of 1.0.

is introduced into db1, or into both db1 and pb1. However, the same substitutions in db2 and/or pb2 do not inhibit cleavage at site 1, and that mutations in all four boxes cause a decrease in overall reactivity of the RNA (Figure 6C, lane 8). We conclude that the two db+pb sets exhibit functional independence, in that an inhibitory base pair in one db+pb set does not adversely affect cleavage directed by the second db+pb set. In this regard it should be noted that an enhancement of cleavage at site 2 is observed when an inhibitory mutation is placed in db1 (Figure 6C, lane 4). This observation suggests that this mutation may cause an equalization in affinity of the two sites for RNase III (see also Discussion).

DISCUSSION

This study has characterized the effects of base pair sequence on the cleavage reactivity and binding affinity of a minimal substrate of *E.coli* RNase III. The properties of μR1.1 RNA as a substrate are relevant in considering the basis for the sequence control of reactivity. The K_m of 148 nM is ~3-fold larger than that of the parent substrate, R1.1 RNA (~50 nM) (40), and the K'_D for the μR1.1 RNA–RNase III complex also is significantly larger than the K'_D values of complexes of RNase III with R1.1 RNA and variants (32,38). The values indicate a relative weak binding affinity. The reduced affinity is consistent with the recent structural analysis of *Aquifex aeolicus* RNase III (D44N mutant), bound to a cleaved RNA (RNA 6) that is identical to the 28 nt product of cleavage of μR1.1 RNA (42). Figure 7B shows the sites of interaction of RNA 6 with specific regions (RBMs) of *A.aeolicus* RNase III. Substrates that are shorter than ~22 bp, such as μR1.1 RNA, would not be able to engage in the full complement of protein contacts (see Figure 7B), and therefore would be expected to have a reduced binding affinity. The protein–RNA contacts observed in the *A.aeolicus* RNase III·RNA 6 cocrystal span ~11 bp (42), which is consistent with the finding that an 11 bp helix between the db and cleavage site is the minimal length needed for significant reactivity. In this regard, the exhaustive cleavage by *E.coli* RNase III of long dsRNAs *in vitro* yields

Table 1. Effect of proximal box substitutions on RNase III binding to μR1.1 RNA

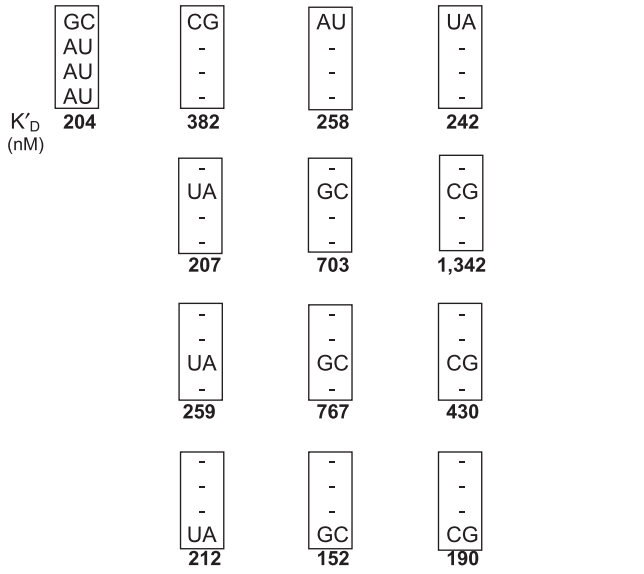

products ranging in size from ~11–15 bp, with negligible amounts of products <~11 bp (7,25,26). The absence of products shorter than 11 bp may in part reflect the low binding affinity of these products, effectively preventing further cleavage.

Figure 7B summarizes the base pair sequence elements that specify a target site for *E.coli* RNase III. The elements are located within an 11 bp helix, and include: (i) the 2 bp db, with a UA and UG pair at positions 1 and 2, respectively; (ii) the 4 bp pb, with a GC pair at pb position 1; an AU or UA pair at pb position 2; an AU pair at pb position 3; and an AU or UA pair at pb position 4; and (iii) a 2 bp segment between the db and pb, termed the middle box (mb), whose sequence content can modulate reactivity (see also below). That a single pb+db set is sufficient to specify an RNase III cleavage site provides additional evidence that the two boxes function as positive recognition determinants. The two target sites in the substrate that contains two db+pb sets exhibit unequal reactivity, with the less reactive site distal to the tetraloop terminus. Mutation of the db for the preferred site yields comparable levels of cleavage at both target sites. These results are consistent with mutually exclusive recognition by RNase III of two sites of unequal affinity. However, further mutational and footprinting analyses are needed to more precisely define the mode of interaction of RNase III with substrates containing multiple overlapping recognition sites.

Evidence that db structure, but not sequence, functions as a positive recognition determinant

The pattern of inhibition by base pair substitutions in the db does not indicate in any obvious manner a direct recognition of sequence by RNase III. Instead, the canonical sequence may provide a unique local structure that is optimally recognized by RNase III. This proposal is supported by hydroxyl radical footprinting and ethylation interference analyses of RNase III–substrate complexes, which show protein contacts with the sugar-phosphate backbone of the db (38). In addition, nucleotide analog interference mapping using substrates containing 2′-deoxyribonucleotide phosphorothioates identified protein contacts with specific 2′-hydroxyl groups within the db (A. Harmouch and A. W. Nicholson, unpublished data). The crystal structure of an *A.aeolicus* RNase III(D44N)•RNA 6 complex (42) reveals the db minor groove as a site of recognition by a segment of the RNase III polypeptide, termed RBM4, that connnects the α5 and α6 helices of the nuclease domain (see Figures 7B and 8). One interaction involves a hydrogen bond between the Arg97 side chain and a ribose 2′-hydroxyl group (42). It is therefore possible that the strong inhibitory effect of the UG→GU substitution (as well as other substitutions) may reflect an alteration of local structure, causing disruption of one or more hydrogen bonds involving the sugar-phosphate backbone and RBM4. In this regard, the UG pair seen in the *A.aeolicus* RNase III(D44N)•RNA 6 cocrystal exhibits the canonical wobble structure, with the attendant local distortion of the double-helix (42).

Additional RNase III side chains may participate in db recognition. The recently-reported crystal structure of *Mycobacterium tuberculosis* RNase III, and molecular modeling analyses (43) suggest a close proximity to the db of a conserved glutamic acid (E100 in *E.coli* RNase III; see Figure 8). It is known that the E100A mutation increases the K_m and k_{cat} for substrates of *E.coli* RNase III (44), and that the E100A mutation (44) as well as the *rnc*-97 (G97E) mutation (45)—both of which map within RBM4—cause a requirement for a higher Mg^{2+} concentration for optimal activity. This suggests that divalent metal ion may either be directly involved in the db-RBM4 interaction, or that it rescues reactivity in an indirect manner. Since RBM4 sequence and length vary among bacterial RNase III orthologs (e.g. see Figure 8), the specific features of the db-RBM4 interaction also may vary across phylogeny, and that the db sequences in turn may be nonconserved. The availability of high-resolution structural data on RNase III–substrate complexes provides a basis to determine the source of specificity and binding energy in db-mediated recognition of substrate.

On the function of the pb as a positive recognition determinant, and as a site of action of catalytic antideterminants

Pb positions 1–3 function as positive recognition determinants for *E.coli* RNase III, with a preferred sequence at each position. In contrast, pb position 4 is a site where specific base pair substitutions can suppress the catalytic step without inhibiting binding. The structure of the *A.aeolicus* RNase III•RNA 6 cocrystal reveals a cluster of hydrogen bonds involving RNA functional groups at pb position 2 and specific side chains in the N-terminal portion of the α8 helix (RBM1) in the dsRBD (Figures 7B and 8) (42). Specifically, the uracil O2 atom in the canonical AU pair and a neighboring ribose 2′-hydroxyl group engage in hydrogen bonds with the Q157 carboxamide group. This interaction suggests a source for the sequence specificity, and also how a purine 2-amino group at pb position 2 could disrupt RNase III

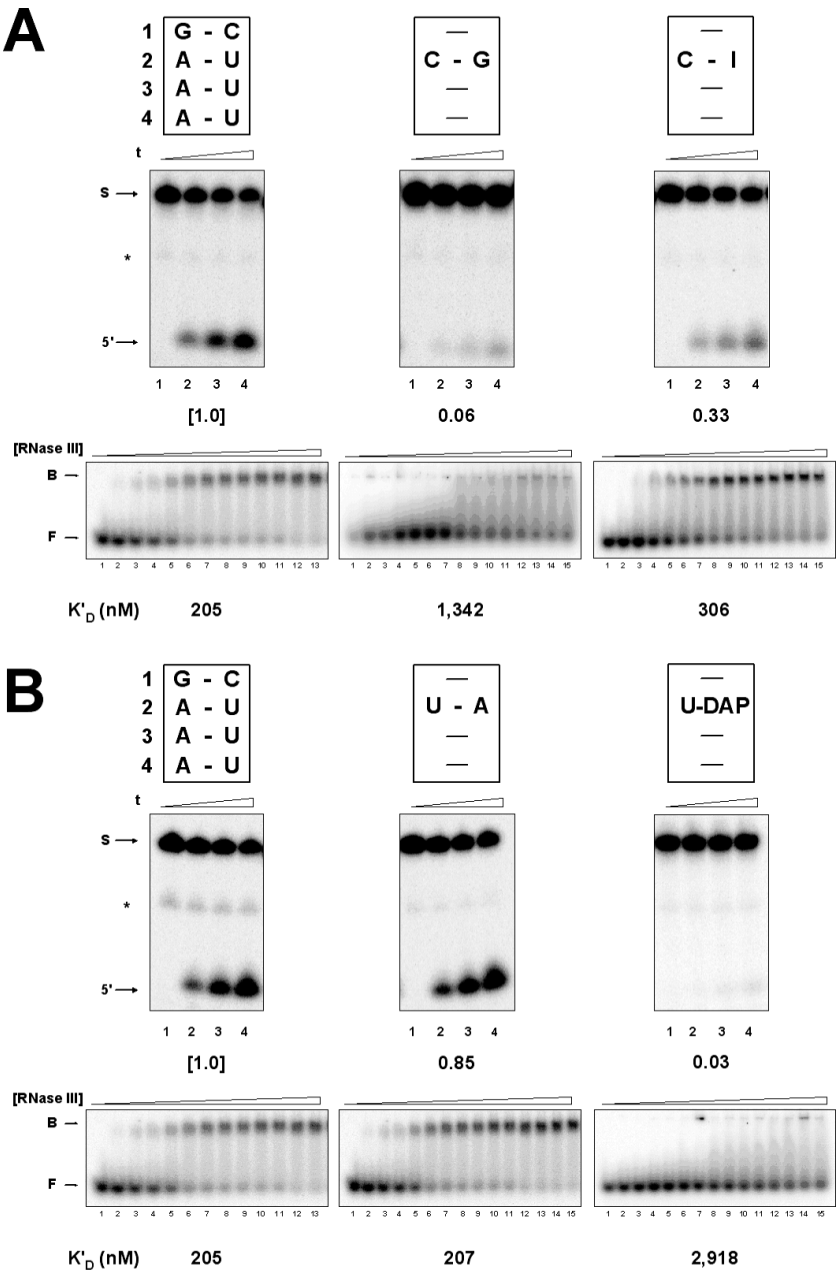

Figure 5. Identification of a minor groove antideterminant. (**A**) Inhibitory effect of the CG bp at the pb second position, and restoration of reactivity upon removal of the 2-amino group (CG→CI bp substitution). The first row shows the sequences; the second row displays the cleavage assays; and the third row displays the gel shift assays. (**B**) Inhibition by DAP substitution. The substrate cleavage assays shown in (A and B) were carried out as described in Materials and Methods, using 5′ ^{32}P-labeled, chemically synthesized RNA. In the cleavage assay gels, lane 1 represents incubation of substrate with RNase III for 4 min in the absence of Mg^{2+}. Lanes 2–4 represent complete reactions, with times of 1, 2.5 and 5 min, respectively. The relative reactivities are provided below the sequences, and represent the averages of at least three independent experiments, with an average standard error of the mean ±10%. 'S' and '5′' indicate the positions of substrate and the 5′ end-containing cleavage product, respectively. The asterisk indicates a product of nonspecific cleavage. For the gel shift assays, lane 1 shows the RNA mobility in the absence of added RNase III. Lanes 2–13 show reactions involving RNase III concentrations of 50, 100, 150, 200, 300, 400, 550, 700, 850, 1000, 1500 and 2500 nM, respectively. Lanes 14 and 15 in panels 2 and 3 involve RNase III concentrations of 3000 and 3500 nM, respectively. 'F' and 'B' indicate the positions of free and bound RNA, respectively. The K'_D values were determined as described in Materials and Methods, and are given below the phosphorimages. The values represent the average of three independent experiments.

recognition. In the latter instance, the inhibitory CG pair would place a 2-amino group (a hydrogen bond donor) adjacent to the Q157 carboxamide amino group (also a hydrogen bond donor). This juxtaposition would not allow hydrogen bond formation, and perhaps also disrupt the hydrogen bond involving the adjacent 2′-hydroxyl group. Moreover, the involvement of two hydrogen bonds rationalizes the ability of the CG→CI substitution to afford only a partial functional rescue. Since the inosine base does not contain a hydrogen bond acceptor group at the C2 position, the Q157 side chain would engage substrate with only a single hydrogen bond. The conservation of the glutamine residue in

RBM1 (Figure 8; A. Pertzev and A. Nicholson, unpublished data) suggests that the Q157 side chain-pb interaction is conserved among RNase III orthologs. It is of interest that RBM1 maps within the dsRBD, whose RNA-binding ability has generally been assumed to be base pair sequence-nonspecific. Ji and coworkers also noted the interaction of specific base functional groups within a bound, non-cleavable dsRNA with the side chains of Q157 and Q161 of *A.aeolicus* RNase III, and the potential for this interaction to provide base pair sequence specificity (20). The apparent ability of the RNase III dsRBD to recognize Watson–Crick base pair sequence at pb position 2 provides the first evidence for the base pair sequence specificity for the dsRBD, and suggests a broadened functional versatility of this motif in mediating dsRNA–protein interactions.

Table 2. Effect of inosine substitution on the uncoupling of binding and cleavage by the GC bp substitution at proximal box position 4

Pb	G – C A – U A – U A – U	-- -- -- G – C	– – – I – C
Relative reactivity	[1.0]	0.09	0.24

Pb position 4 represents a separate locus of protein interaction. Here, a ribose 2′-hydroxyl group and a non-bridging phosphate oxygen engage in hydrogen bonds with the side chains of specific residues in the α4 helix, termed RBM3 (42) (see Figures 7B and 8). No base-specific contacts are observed. The ability of the GC or CG substitution at pb position 4 to suppress cleavage without inhibiting substrate binding formally classifies these sequences as catalytic antideterminants (29). While the mechanism of inhibition is not known, one possibility is that a substrate conformational

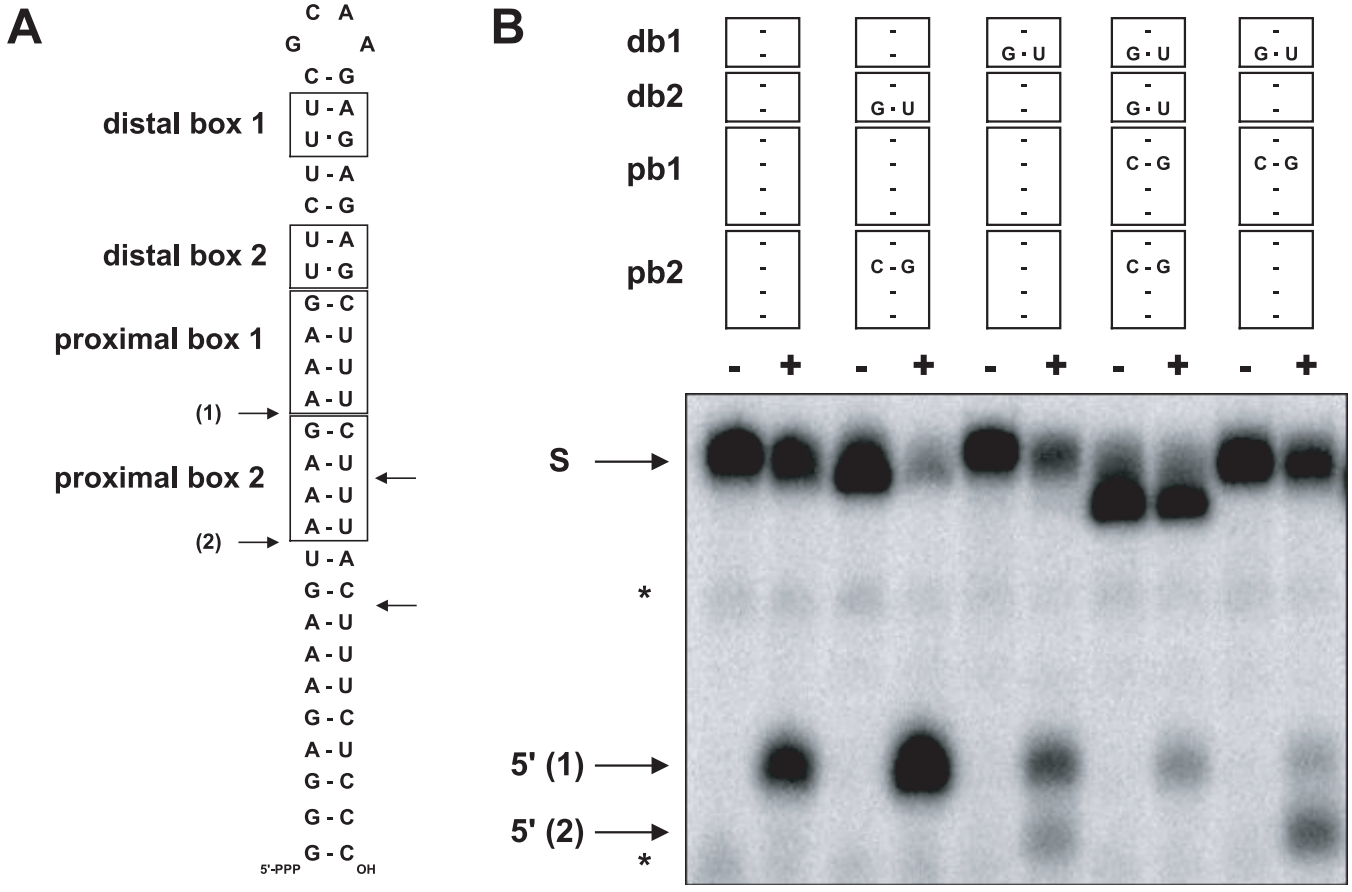

Figure 6. RNase III cleavage of a substrate containing two pb+db sets. (**A**) Structure of R1.1[db1pb1,db2pb2) RNA. (**B**) Cleavage reactivities of R1.1[db1pb1,db2pb2] RNA and several variants. The base pair substitutions in the proximal and/or dbs are indicated. Cleavage assays were performed using 5′ ^{32}P-labeled RNA (~2.5 nM), in standard reaction buffer (see Materials and Methods). For each substrate, the first lane represents incubation of the RNA for 4 min with RNase III (10 nM dimer concentration) in the absence of Mg^{2+}. The second lane represents the complete reaction (including 10 mM Mg^{2+}), incubated for 2.5 min. Reactions were analyzed by electrophoresis in a 15% polyacrylamide gel and visualized by phosphorimaging as described in Materials and Methods. The positions of the 5′ ^{32}P-labeled products [5′ (1) and 5′ (2)], and the uncleaved substrate (S) are indicated. The asterisks indicate two fragments resulting from a nonenzymatic cleavage reaction, and which also were present in the control reactions that lacked Mg^{2+}. The cleavage sites were identified in separate experiments by comparison of product fragment migration with that of the cleavage products of R1.1[WC] RNA, and also by sequencing gel analysis, using a P1 nuclease ladder (G>A-specific) (55), an RNase T1 ladder (G-specific) and an alkaline ladder (gel electropherograms not shown). The corresponding 3′ end-containing cleavage products, and internal fragments are not visible, since the RNAs are 5′ ^{32}P-labeled. However, these species are observed when internally-labeled (A,U) RNA is used as substrate (gel electropherograms not shown). The altered mobility of the uncleaved substrates reflects the differing GC bp content of the variants, which affects electrophoretic mobility in the presence of 7 M urea. This mobility difference has been observed elsewhere (32).

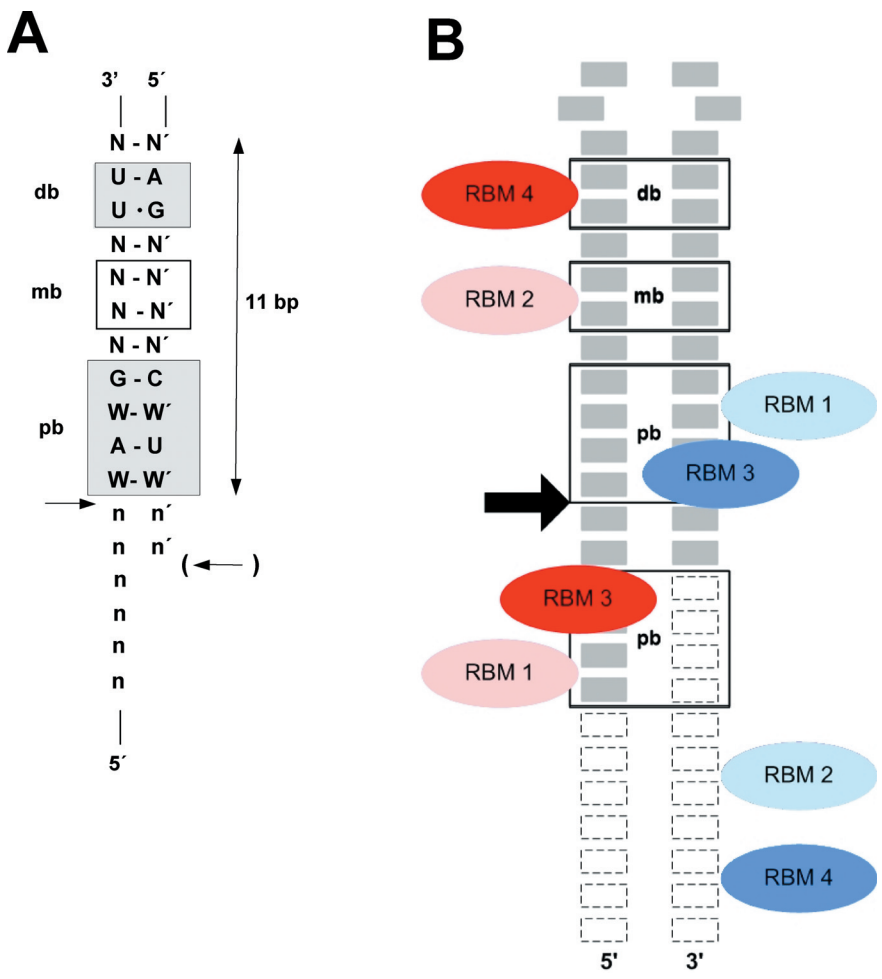

Figure 7. Consensus sequence elements of an *E.coli* RNase III substrate, and sites of interaction of the db, pb and mb with RNase III. (**A**) Consensus sequence elements that specify an *E.coli* RNase III cleavage site. The consensus base pair sequence elements were established by excluding the base pair substitutions that reduce cleavage reactivity by >2-fold (i.e. a relative reactivity <~0.5; see Figure 3). N, n: any nucleotide; N-N′ indicates a relatively strict requirement for Watson–Crick base pairing, while n–n′ indicates a minimal requirement for base pairing. W-W′: AU or UA bp. The arrows indicate the scissile phosphodiesters. The parentheses flanking the right arrow indicate that this cleavage site is not a required feature, but would be recognized if the 3′ end of the RNA were extended beyond this site. (**B**) Diagram, based on Figure 5 in (42), showing contacts of the db, mb and pb with RBMs 1–4 of a bacterial (*A.aeolicus*) RNase III. The location of each RBM in the RNase III holoenzyme is indicated by a specific color. The pink and red colors denote the motifs of one subunit, while the blue and aqua colors denote the motifs of the other subunit. In each case, the lighter color indicates that the motif is located in the dsRBD, while the darker color indicates that the motif is located in the nuclease domain (see Figure 8). The position of bound μR1.1 RNA is indicated by the grey rectangles, with each rectangle representing a nucleotide. The rectangles with dashed outlines indicate the positions of the nucleotides of a full-length substrate bound to RNase III. Note the absence of two RBM contacts in the μR1.1 RNA–RNase III complex. The arrow indicates the RNase III cleavage site.

change required for cleavage may be hindered by the stronger GC or CG bp. Consistent with this proposal, substitution of guanine by inosine lessens the inhibition caused by the GC bp substitution. However, since reactivity is not fully restored, other features unique to the GC/CG bp apparently participate in the uncoupling of binding and cleavage. It is noteworthy that R1.1[CL3B] RNA—a cleavage-resistant, but binding-competent R1.1 RNA variant identified by *in vitro* selection (29)—contains a GC pair at pb position 4, while the efficiently cleaved R1.1 RNA contains a nominally stable UC pair at the same position (40,46). Catalytic antideterminants have been identified in substrates of the yeast RNase III ortholog, Rnt1p (47–49). It was shown in one of the studies that a UA bp substitution at the tetraloop closing position uncouples binding and cleavage, and that the adenine 6 amino group is specifically responsible for uncoupling (49). The ability of Watson–Crick base pairs to function as catalytic antideterminants suggests that regular double-helical structures can provide cleavage-resistant binding sites for RNase III, with potential gene-regulatory functions.

Modulation of reactivity by a double-helical element between the pb and db

The sequence content of a 2 bp segment between the db and pb modulates substrate reactivity. Here, the U_{12}:G_{27}→GU or GC substitution enhances cleavage reactivity (relative reactivity of 1.4), while the C_{13}:G_{26}→GC substitution decreases reactivity (relative reactivity of 0.36) (Figure 3). The structure of the *A.aeolicus* RNase III–RNA complex reveals that this segment, termed the middle box (mb) (42), is a site of

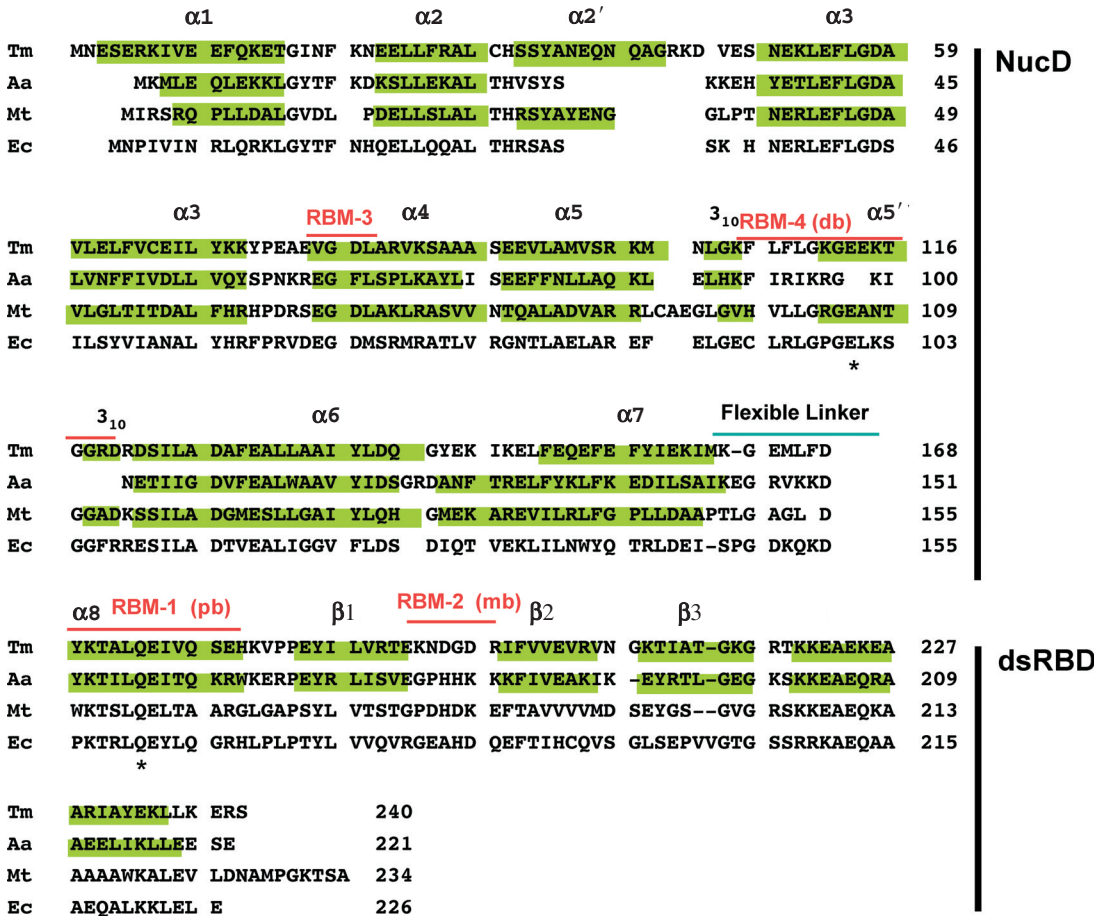

Figure 8. Locations of RBMs 1–4 in bacterial RNase III polypeptides. Shown is a sequence alignment of four bacterial RNase III polypeptides, indicating the locations of secondary structural elements (highlighted in green) as determined by X-ray crystallography, and also the positions of RBMs 1–4. Noted by each motif is the site of interaction with the minimal substrate (pb, db or mb), as provided by the crystallographic analysis of *A.aeolicus* (Aa) RNase III bound to a cleaved minimal substrate (42). The secondary structural elements for Aa RNase III and *M.tuberculosis* (Mt) RNase III were from (42,43), respectively. The secondary structure of the dsRBD of Mt RNase III is not shown, since the position of the dsRBD is disordered in the crystal (43). The secondary structural elements of *Thermotoga maritima* (Tm) RNase III were provided by the Joint Center for Structural Genomics (San Diego) (PDB entry 1O0W). The secondary structure of *E.coli* (Ec) RNase III is not known, since the structure of the protein has not been determined. The nuclease domain (NucD), dsRBD, and flexible linker regions are noted. The asterisks indicate conserved residues within RBM1 and RBM4 that interact with the pb and db, respectively (see also Discussion).

protein contact. Specifically, a ribose 2′-hydroxyl group in the mb engages in a hydrogen bond with the side chain of a Histidine (H180) residue within the segment, termed RBM2, that connects the β1 and β2 strands of the dsRBD (42) (see Figures 7B and 8). The lack of strong inhibition by Watson–Crick base pair substitutions supports the absence of base-specific contacts. However, it is possible that certain substitutions (e.g. non-Watson–Crick base pairs) that alter local structure could control reactivity by determining whether the observed hydrogen bond is established, and thus serve to 'fine-tune' substrate reactivity.

SUMMARY

It was originally proposed that *E.coli* RNase III cleavage sites are identified by a default pathway, wherein specifically positioned Watson–Crick base pair antideterminants mask otherwise reactive phosphodiesters, thereby limiting cleavage to a single target site (3,32). The model did not require the involvement of positive recognition determinants. This study has allowed a refinement of the model to include positive recognition determinants in the form of specific base pair sequences. Thus, both positive as well as negative (i.e. antideterminant) elements cooperate to identify the cleavage site(s) and control reactivity of *E.coli* RNase III substrates, and by extension other bacterial RNase III substrates. The ability of base pair sequence to modulate reactivity can serve to establish hierarchical reactivities among the diverse array of cellular substrates. Thus, the binding affinity can determine cleavage efficiency, that in turn can establish the RNA decay rate, if RNase III action represents the rate-limiting event in a multi-step pathway. Finally, given the growing number of characterized substrates for eukaryotic RNase III orthologs (50,51), and the identification of functionally essential RNase III polypeptides in kinetoplastid RNA editosomes (52,53) it can be anticipated that base pair sequence control of RNase III action may be operative in RNA processing and decay pathways in eukaryotic cells.

ACKNOWLEDGEMENTS

This paper is dedicated to the memory of Hugh D. Robertson, a pioneer in research on RNA processing. The authors thank Xinhua Ji and Don Court for sharing results prior to publication and for informative discussions. The authors also thank Rhonda Nicholson for comments on the manuscript, Wenzhao Meng for help with Figure 7, and other members of the laboratory for their advice and support. This research was supported by NIH grants GM56772 and GM56457. Funding to pay the Open Access publication charges for this article was provided by Temple University.

Conflict of interest statement. None declared.

REFERENCES

1. D'Alessio,G. and Riordan,J.F. (eds) (1997) *Ribonucleases: Structures and Functions*. Academic Press, NY.
2. Belasco,J.G. and Brawerman,G. (eds) (1993) *Control of Messenger RNA Stability*. Academic Press, NY.
3. Nicholson,A.W. (1999) Function, mechanism and regulation of bacterial ribonucleases. *FEMS Microbiol. Rev.*, **23**, 371–390.
4. Deutscher,M.P. and Li,Z. (2001) Exoribonucleases and their multiple roles in RNA metabolism. *Prog. Nucleic Acids Res. Mol. Biol.*, **66**, 67–105.
5. Carpousis,A.J. (2002) The *Escherichia coli* RNA degradosome: structure, function and relationship to other ribonucleolytic multienzyme complexes. *Biochem. Sci. Trans.*, **30**, 150–155.
6. Meyer,S., Temme,C. and Wahle,E. (2004) Messenger RNA turnover in eukaryotes: pathways and enzymes. *CRC Crit. Rev. Mol. Biol.*, **39**, 197–216.
7. Court,D.L. (1993) RNA processing and degradation by RNase III. In Belasco,J.G. and Brawerman,G. (eds) *Control of Messenger RNA Stability*. Academic Press, NY. pp. 71–116.
8. LaMontagne,B., Larose,S., Boulanger,J. and AbouElela,S. (2001) The RNase III family: a conserved structure and expanding functions in eukaryotic dsRNA metabolism. *Curr. Issues Mol. Biol.*, **3**, 71–78.
9. Nicholson,A.W. (2003) The ribonuclease III superfamily: forms and functions in RNA maturation, decay, and gene silencing. In Hannon,G.J. (ed.), *RNAi: A Guide to Gene Silencing*. Cold Spring Harbor Laboratory Press, Cold Spring Harbor, NY, pp. 149–174.
10. Carmell,M.A. and Hannon,G.J. (2004) RNase III enzymes and the initiation of gene silencing. *Nature Struct. Mol. Biol.*, **11**, 214–218.
11. Drider,D. and Condon,C. (2004) The continuing story of endoribonuclease III. *J. Mol. Microbiol. Biotechnol.*, **8**, 195–200.
12. Bernstein,E., Caudy,A.A., Hammond,S.M. and Hannon,G.J. (2001) Role for a bidentate ribonuclease in the initiation step of RNA interference. *Nature*, **409**, 363–366.
13. Zhang,H., Kolb,F.A., Jaskiewicz,L., Westhof,E. and Filipowicz,W. (2004) Single processing center models for human Dicer and bacterial RNase III. *Cell*, **118**, 57–68.
14. MacRae,I.J., Zhou,K., Li,F., Repic,A., Brooks,A.N., Cande,W.Z., Adams,P.D. and Doudna,J.A. (2006) Structural basis for double-stranded RNA processing by Dicer. *Science*, **311**, 195–198.
15. Lee,Y., Ahn,C., Han,J., Choi,H., Kim,J., Yim,J., Lee,J., Provost,P., Radmark,O., Kim,S. *et al.* (2003) The nuclear RNase III Drosha initiates microRNA processing. *Nature*, **425**, 415–419.
16. Zeng,Y. and Cullen,B.R. (2005) Efficient processing of primary microRNA hairpins by Drosha requires flanking non-structured RNA sequences. *J. Biol. Chem.*, **280**, 27595–27603.
17. Hutvagner,G., McLachlan,J., Pasquinelli,A.E., Balint,E., Tuschl,T. and Zamore,P.D. (2001) A cellular function for the RNA-interference enzyme Dicer in the maturation of the let-7 small temporal RNA. *Science*, **293**, 834–838.
18. Ketting,R.F., Fischer,S.E.J., Bernstein,E., Sijen,T., Hannon,G.J. and Plasterk,R.H.A. (2001) Dicer functions in RNA interference and in synthesis of small RNA involved in developmental timing in *C. elegans*. *Genes Dev.*, **15**, 2654–2659.
19. Blaszczyk,J., Tropea,J.E., Bubnenko,M., Routzahn,K.M., Waugh,D.S., Court,D.L. and Ji,X. (2001) Crystallographic and modeling studies of RNase III suggest a mechanism for double-stranded RNA cleavage. *Structure (Camb.)*, **9**, 1225–1236.
20. Blaszczyk,J., Gan,J., Tropea,J.E., Court,D.L., Waugh,D.S. and Ji,X. (2004) Noncatalytic assembly of ribonuclease III with double-stranded RNA. *Structure (Camb.)*, **12**, 457–466.
21. Saunders,L.R. and Barber,G.N. (2003) The dsRNA binding protein family: critical roles, diverse cellular functions. *FASEB J.*, **17**, 961–983.
22. Doyle,M. and Jantsch,M.F. (2003) New and old roles of the double-stranded RNA-binding domain. *J. Struct. Biol.*, **140**, 147–153.
23. Tian,B., Bevilacqua,P.C., Diegelman-Parente,A. and Mathews,M.B. (2004) The double-stranded-RNA-binding motif: interference and much more. *Nature Rev. Mol. Biol.*, **5**, 1013–1023.
24. Chang,K.-Y. and Ramos,A. (2005) The double-stranded RNA-binding motif, a versatile macromolecular docking platform. *FEBS J.*, **272**, 2109–2117.
25. Robertson,H.D. (1982) *Escherichia coli* ribonuclease III cleavage sites. *Cell*, **30**, 669–672.
26. Dunn,J.J. (1982) Ribonuclease III. In Boyer,P.D. (ed.), *The Enzymes*. Academic Press, NY, pp. 485–499.
27. Franch,T. and Gerdes,K. (1999) Ribonuclease III processing of coaxially stacked RNA helices. *J. Biol. Chem.*, **274**, 26572–26578.
28. Dunn,J.J. and Studier,F.W. (1983) Complete nucleotide sequence of bacteriophage T7 and the locations of T7 genetic elements. *J. Mol. Biol.*, **166**, 477–535.
29. Calin-Jageman,I. and Nicholson,A.W. (2003) RNA structure-dependent uncoupling of substrate recognition and cleavage by *Escherichia coli* ribonuclease III. *Nucleic Acids Res.*, **31**, 2381–2392.
30. Altuvia,S., Locker-Giladi,H., Koby,S., Ben-Nun,O. and Oppenheim,A.B. (1987) RNase III stimulates the translation of the cIII gene of bacteriophage lambda. *Proc. Natl Acad. Sci. USA*, **84**, 6511–6515.
31. Krinke,L. and Wulff,D.L. (1990) The cleavage specificity of RNase III. *Nucleic Acids Res.*, **18**, 4809–4815.
32. Zhang,K. and Nicholson,A.W. (1997) Regulation of ribonuclease III processing by double-helical sequence antideterminants. *Proc. Natl Acad. Sci. USA*, **94**, 13437–13441.
33. He,B., Rong,M., Lyakhov,D., Gartenstein,H., Diaz,G., Castagna,R., McAllister,W.T. and Durbin,R.K. (1997) Rapid mutagenesis and purification of phage RNA polymerases. *Prot. Expr. Purif.*, **9**, 142–151.
34. Amarasinghe,A.K., Calin-Jageman,I., Harmouch,A., Sun,W. and Nicholson,A.W. (2001) *Escherichia coli* ribonuclease III: affinity purification of hexahistidine-tagged enzyme and assays for substrate binding and cleavage. *Meth. Enzymol.*, **342**, 143–158.
35. Pokrovskaya,I.D. and Gurevich,V.V. (1994) *In vitro* transcription: preparative RNA yields in analytical scale reactions. *Anal. Biochem.*, **220**, 420–423.
36. Milligan,J.F., Groebe,D.R., Witherell,G.W. and Uhlenbeck,O.C. (1987) Oligoribonucleotide synthesis using T7 RNA polymerase and synthetic DNA templates. *Nucleic Acids Res.*, **15**, 8783–8798.
37. Richards,E.G. (1975) Nucleic Acids. In Fasman,G.D. (ed.), *Handbook of Biochemistry and Molecular Biology*. CRC Press, Cleveland, OH, p. 597.
38. Li,H. and Nicholson,A.W. (1996) Defining the enzyme binding domain of a ribonuclease III processing signal. Ethylation interference and hydroxyl radical footprinting using catalytically inactive RNase III mutants. *EMBO J.*, **15**, 1421–1433.
39. Carey,J. (1991) Gel retardation. *Meth. Enzymol.*, **208**, 103–117.
40. Chelladurai,B.S., Li,H., Zhang,K. and Nicholson,A.W. (1993) Mutational analysis of a ribonuclease III processing signal. *Biochem.*, **32**, 7249–7558.
41. Jucker,F.M., Heus,H.A., Yip,P.F., Moors,E.H. and Pardi,A. (1996) A network of heterogeneous hydrogen bonds in GNRA tetraloops. *J. Mol. Biol.*, **264**, 968–980.
42. Gan,J., Tropea,J.E., Austin,B.P., Court,D.L., Waugh,D.S. and Ji,X. (2006) Structural insight into the mechanism of double-stranded RNA processing by ribonuclease III. *Cell*, **124**, 355–366.
43. Akey,D.L. and Berger,J.M. (2005) Structure of the nuclease domain of ribonuclease III from *M. tuberculosis* at 2.1 Å. *Protein Sci.*, **14**, 2744–2750.

44. Sun,W., Li,G. and Nicholson,A.W. (2004) Mutational analysis of the nuclease domain of *Escherichia coli* ribonuclease III. Identification of conserved acidic residues that are important for catalytic function *in vitro*. *Biochem.*, **43**, 13054–13062.
45. Davidov,Y., Rahat,A., Flechner,I. and Pines,O. (1993) Characterization of the *rnc*-97 mutation of RNase III: a glycine to glutamate substitution increases the requirement for magnesium ions. *J. Gen. Microbiol.*, **139**, 717–724.
46. Calin-Jageman,I. and Nicholson,A.W. (2003) Mutational analysis of an RNA internal loop as a reactivity epitope for *Escherichia coli* ribonuclease III. *Biochem.*, **42**, 5025–5034.
47. Lamontagne,B., Ghazal,G., Lebars,I., Yoshizawa,S., Fourmy,D. and AbouElela,S. (2003) Sequence dependence of substrate recognition and cleavage by yeast RNase III. *J. Mol. Biol.*, **327**, 985–1000.
48. Lamontagne,B. and AbouElela,S. (2004) Evaluation of the RNA determinants for bacterial and yeast RNase III binding and cleavage. *J. Biol. Chem.*, **279**, 2231–2241.
49. Sam,M., Henras,A.K. and Chanfreau,G. (2005) A conserved major groove antideterminant for *Saccharomyces cerevisiae* RNase III recognition. *Biochem.*, **44**, 4181–4187.
50. Haussecker,D. and Proudfoot,N.J. (2005) Dicer-dependent turnover of intergenic transcripts from the human beta-globin gene cluster. *Mol. Cell. Biol.*, **25**, 9724–9733.
51. Rose,S.D., Kim,D.H., Amarzguioui,M., Heidel,J.D., Collingwood,M.A., Davis,M.E., Rossi,J.J. and Behlke,M.A. (2005) Functional polarity is introduced by Dicer processing of short substrate RNAs. *Nucleic Acids. Res.*, **33**, 4140–4156.
52. Carnes,J., Trotter,J.R., Ernst,N.L., Steinberg,A. and Stuart,K. (2005) An essential RNase III insertion editing endonuclease in *Trypanosoma brucei*. *Proc. Natl Acad. Sci. USA*, **102**, 16614–16619.
53. Trotter,J.R., Ernst,N.L., Carnes,J., Panicucci,B. and Stuart,K. (2005) A deletion site editing endonuclease in *Trypanosoma brucei*. *Mol. Cell*, **20**, 403–412.
54. Carey,J., Cameron,V., deHaseth,P.L. and Uhlenbeck,O.C. (1983) Sequence-specific interaction of R17 coat protein with its ribonucleic acid binding site. *Biochem.*, **22**, 2601–2610.
55. Cruz-Reyes,J., Piller,K.J., Rusche,L.N., Mukherjee,M. and Sollner-Webb,B. (1998) Unexpected electrophoretic migration of RNA with different 3′-termini causes a RNA sizing ambiguity that can be resolved using nuclease P1-generated sequencing ladders. *Biochem.*, **37**, 6059–6064.